Chapter 9

Diluted Magnetic DNA Nanowires

Caner Değer, Vahap Eldem and İzzet Paruğ Duru

Additional information is available at the end of the chapter

http://dx.doi.org/10.5772/67921

Abstract

DNA, as a natural biological nanowire, could be modified by inorganic atoms, either conducting or semi-conducting ones, to render feasible for technological applications and sequencing. Magnetic phase transition of modified DNA (M-DNA) nanowire, similar to diluted magnetic semiconductor (DMS) materials, occurs by changing parameters such as temperature and doping ratio having critical values. Tuning such parameters provide a pleasant control about determination of the magnetic property of M-DNA, particularly room-temperature soft ferromagnetism. In this chapter, a fundamental theory for anti-ferromagnetic Cr^{3+}-doped M-DNA nanowire named as diluted magnetic organic structures (DMOS) is tried to figure out the interactions representing the exotic behaviour of these type of organometallics. However, authors detailed preparation of nanowire as a global input and overall procedure of simulation based on Markov chain Monte Carlo (MCMC) method.

Keywords: DMOS, M-DNA, dipolar Interaction, hysteresis, organic nanowire, MCMC

1. Introduction

With unique structural features and self-assembly nature, deoxyribonucleic acid (DNA) has long been considered as ubiquitous bionanomaterials. The unique structural patterns and dynamic behaviours of DNA mainly arise from hydrogen bonds between purine and pyrimidine bases which are fundamental building blocks in double helix. Moreover, the editable, modifiable, scalable, and controllable natures of polynucleotides make synthetic DNA an attractive material for several applications at the nanoscale fields, including optoelectronics [1], spintronics [2], nanophotonics [3], nanobiosensors [4, 5] and even data storages such as nucleic acid memory. On the other hand, despite all these advantages,

optical, electronic and magnetic properties of bare DNA are not suitable for such applications. Therefore, by doping DNA with divalent metal ions (Cu^{2+}, Ni^{2+}, Zn^{2+}, and Co^{2+}), called "modified DNA (M-DNA)", it is possible to tailor or control the magnetic and electrical properties of DNA. Besides, changing magnetic property of DNA via selective incorporation of metal ions between purine-pyrimidine pairs and hydrogen bonds not only provides a tunable material but also gives a clue about the location of bases. However, Hu et al. [6] investigated the electronic and magnetic properties of graphene and Fe and probe the DNA bases adsorbed by first-principal calculations theoretically to detect DNA bases. As a matter of fact, researchers recently focused on conceiving magnetic properties of M-DNA nanowires even though Azbel [7] derived an explicit formula that provides the consistency of theory and experiments while studying phase transitions in DNA. Alivisatos et al. [8], Mirkin et al. [9], and Braun et al. [10] were the first researchers who studied DNA-templated self-assembly, followed by Richter et al. [11], Park et al. [12] and Keren et al. [13]. Fabrication of DNA nanowires extend the field of workspace generated by organic structures. Park et al. [12] studied detection of nucleic acids with high sensitivity and specificity. Besides fabrication of DNA nanowires, band-gap effects on temperature-dependent magnetism of DNA molecules have been evaluated by Yi [14]. On the other hand, Savin et al. [15] described the thermal properties of DNA, especially heat conductivity of the DNA double helix, constructing a 3D coarse-grain (CG) model. Therefore, some studies have been carried out to reveal magnetic properties of M-DNA, both theoretically and experimentally. Electronic states of metal ion-doped M-DNA (m is Mn, Ni, Mg, Co and Fe) are figured out by optical absorption concluding charge transfer from Fe^{2+} to DNA and transferred charges should be positioned close to bases [16]. Computational models are properly developed to investigate the electrical conduction in DNA nanowires by Panahi and Chitsazanmoghaddam [17] and Behnia and Fathizadeh [18]. The studies performed by Dugasani et al. [19] and Nikiforov et al. [20] discovered that divalent metal ion–doped DNA exhibits soft ferromagnetic (FM) behaviour. Both of the studies claim that the origin of the soft ferromagnetic behaviour is the interaction between doped ions. Long-range interactions have also been proposed as the cause of room-temperature ferromagnetism in M-DNA. On the other hand, a comprehensive theoretical study proposed a new type of Hamiltonian approach suggesting both inorganic and organic structures including M-DNA nanowires [21]. One of the significant terms of Hamiltonian indicates exchange interaction, the ferromagnetic or anti-ferromagnetic interaction between atoms. The effect of ion concentration on the system was investigated to determine the proper ratio for technological applications. The result of the study is also compatible with experimental studies.

2. Constructing modified DNA nanowires

In this section, a simple workflow is introduced for construction of the modified DNA structure doped by a metal ion (Cr^{3+}) to investigate magnetic properties, especially soft ferromagnetism related to doping ratio. Firstly, a set of gene sequences should be designated as a sample group considering the guanine-cytosine (G-C)% content and base composition herewith sequence length. It is important to know the base composition of DNA and the number

of hydrogen bounds since dopant ion is replaced with hydrogen atoms. After the determination of sample group (base sequences), base pairs containing organic atoms will be converted to a 3D structure by assigning atomistic coordinates of atoms in Euclidian space. van Dijk and Bonvin [22] developed a model to produce atomistic coordinates with connections of atoms from the singe base sequence of a gene in the mentioned coordinate space using reasonable parameters. The key parameters are roll, tilt and twist during the modelling procedure combined with each other. By the usage of 3D DART modelling tool [23], resulting DNA helical was ready to be modified by a dopant ion. Doping process is required to start after the successful finish of former work. Dugasani et al. [19] suggested the most probable locations of subsequent dopant ions between base pairs and PO4, and at last, the random displacement of dopants instead of hydrogen atoms of N-H-N and N-H-O.

2.1. Preparation of the sample group

G-C base pair has three electrostatic hydrogen bonds between nitrogen and oxygen atoms, while adenine-thymine (A-T) base pairs are connected to each other via two hydrogen bonds in the Watson-Crick model. Duru et al. [21] doped a number of genes with length of 1000 bases whose G-C ratio ranged from 40.8 to 69.5%. Sample group prepared has hydrogen bonds between the G and C bases ranging from 1124 to 2085 and the ratio of A to T content ranging from 610 to 1184. Authors prepared a sample group having different genes and G-C contents to re-simulate the M-DNA. The sample sequences of DNA (1000 bases) in length were obtained from Ensembl Genome browser (www.ensembl.org). Detailed information about the base composition of selected genes is presented in **Table 1**.

2.2. Atomistic structure of DNA

Polynucleotide chains constitute DNA by helical circling which is either right handed or left handed. As the most common form, B-DNA is right handed. There are a major groove and a minor groove through the outer region, respectively. Yet another right-handed helical A-DNA is a more congested molecule. Contrary to A-DNA and B-DNA, Z-DNA is a left-handed helical DNA. Base pairs are seen as zigzags. Moreover, helical structure forms a deep indentation instead of two. The Watson-Crick model, B-DNA, is considered as the normal form. The model is for the damp form due to the high water activity in vivo. That model has 10 base pairs per turn of the double helix, with a rise of 3.4 Å/bp [24], and A-DNA has 11 base pairs per turn and a rise of 2.6 Å/bp [25]. **Table 2** compares some properties of A-DNA, B-DNA and Z-DNA.

Sequences of all genes of the sample group should be used to visualize the atomic coordinates using U-GENE (free open-source cross-platform) separately (can be downloaded from http://ugene.net/). All of the atoms have the same spherical geometry. First, distances between the first 10 nearest neighbours of all atoms in DNA are calculated to provide a reasonable process time during simulation. van Dijk et al. [22] proposed a method to generate a canonical structure including atomic positions of A-DNA and B-DNA. The modelling procedure is clearly detailed in their work. B-DNA should be preferred for simulation process due to the most observed structural form of bare DNA in vivo.

Gene name	Length (bp)	A (%)	T (%)	G (%)	C (%)	%GC	M.W. (Da)
ADGB[a]	1000	32.8	26.4	17.1	23.7	40.8	312,051
AGRN[b]	1000	15.1	15.4	34.7	34.8	69.5	312,177
AK1[c]	1000	25	18.2	24.2	32.6	56.8	313,148
ALB[d]	1000	29.2	28.2	19.8	22.8	42.6	311,340
FOXA1[e]	1000	19.7	13	35.5	31.8	67.3	311,793
MFN1[f]	1000	30.3	27.4	17.6	24.7	42.3	312,046
PODN[g]	1000	21	17.3	33.5	28.2	61.7	311,130
SMOX[h]	1000	21.9	18.8	29.2	30.1	59.3	311,944
SMTN[j]	1000	21.2	14.1	33.4	31.3	64.7	311,929
TESK1[k]	1000	18.6	18.8	31.1	31.5	62.6	311,883

[a] androglobin
[b] agrin
[c] adenylate kinase 1
[d] albumin
[e] forkhead box A1
[f] mitofusin 1
[g] podocan
[h] spermine oxidase
[j] smoothelin
[k] testis-specifc kinase 1 [21].

Table 1. List of genes with different base compositions and molecular weights (M.W.).

	A-DNA	B-DNA	Z-DNA
Helix sense	right-handed	right-handed	left-handed
Repeating unit	1	1	2
Rotation/bp	32.7°	34.3°	60°/2
Inclination of bp to axis	+19°	−1.2°	−9°
Rise/bp along axis	0.26 nm	0.34 nm	0.37 nm
Rise/turn of helix	2.86 nm	3.57 nm	4.56 nm
Mean propeller twist	+18°	+16°	0°
Nucleotide phosphate to phosphate distance	0.59 nm	0.70 nm	C: 0.57 nm, G: 0.61 nm
Diameter	2.3 nm	2.0 nm	1.8 nm

Table 2. Comparing geometries of A-DNA, B-DNA and Z-DNA.

Figure 1 shows A-T and G-C base pairs, including base atoms having spherical geometry and bounds roughly. Furthermore, the flow diagram of the distance calculated between nearest neighbours is given by **Figure 2**. Finalization process of preparing input data would be followed by the doping process explained in the next section.

http://dx.doi.org/10.5772/67921

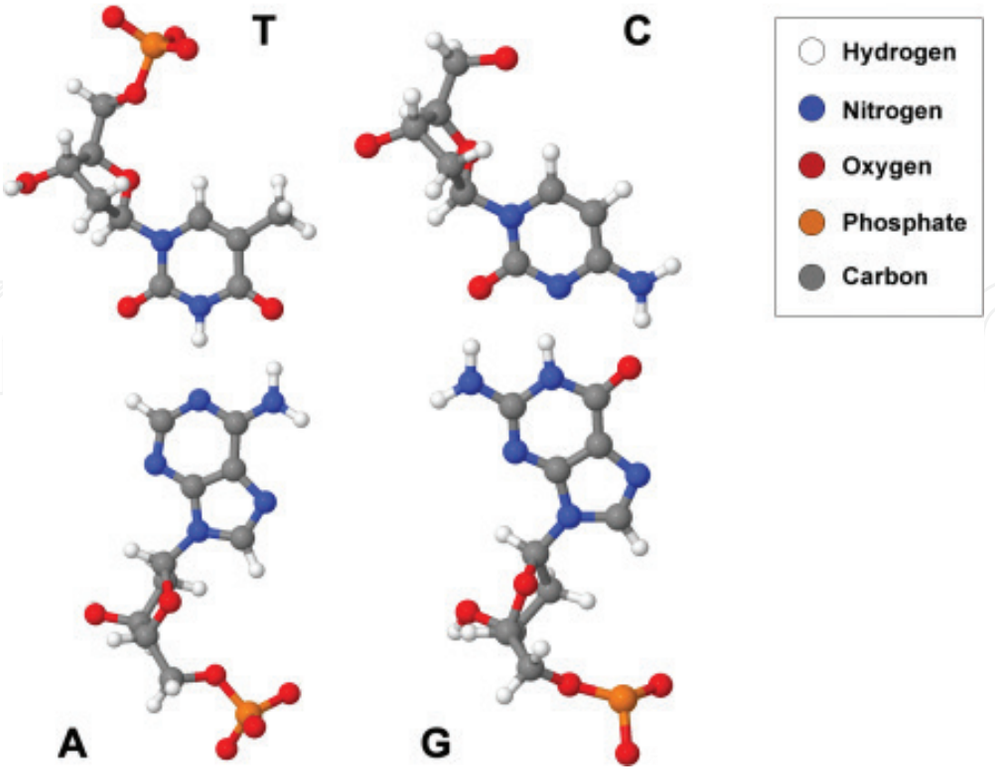

Figure 1. A molecular structure of A-T and C-G base pairs.

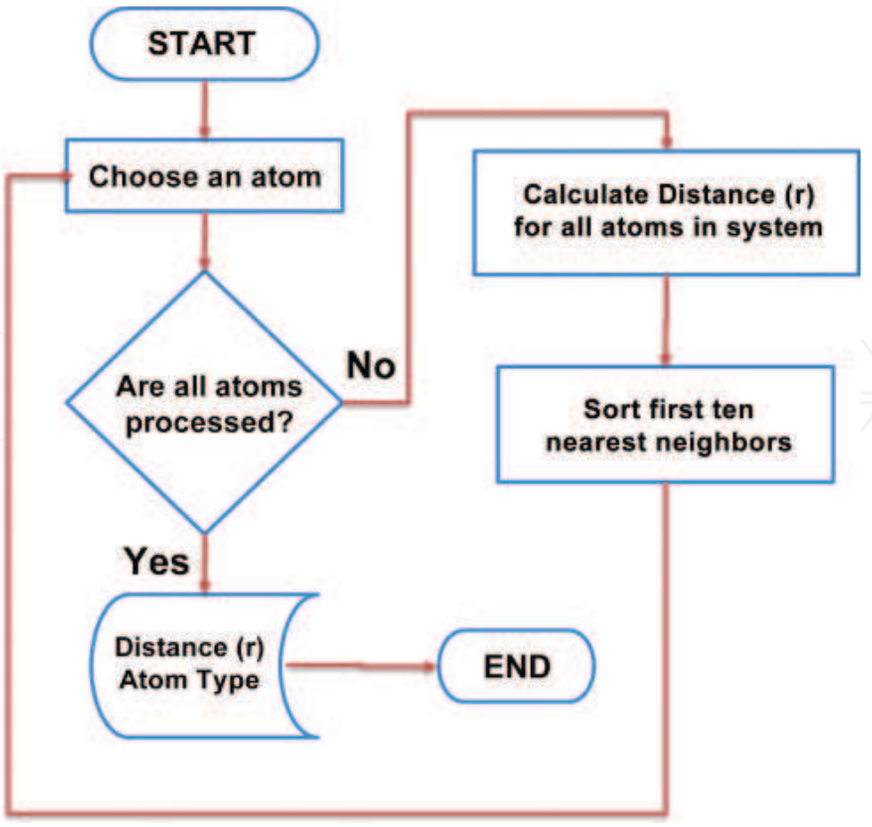

Figure 2. A flow diagram of first 10 nearest neighbours' distance calculation.

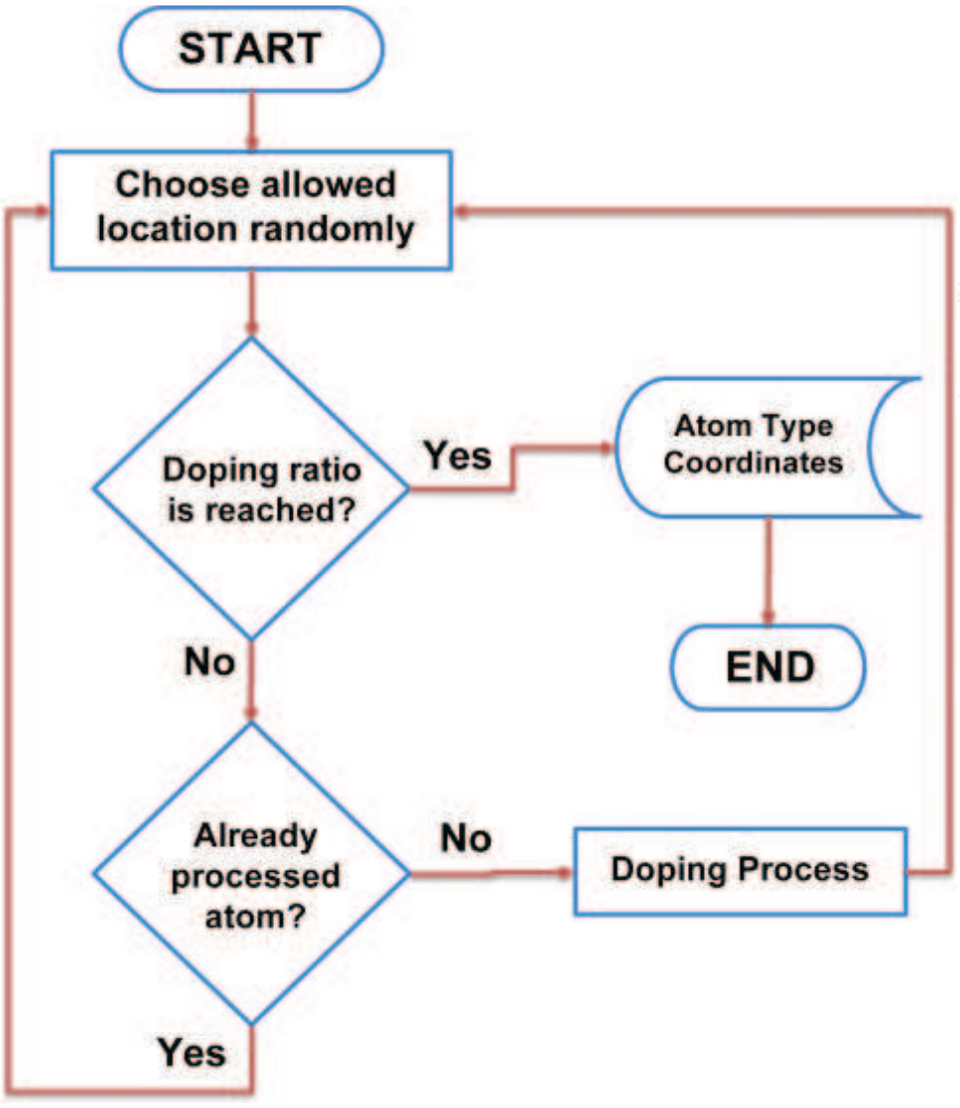

Figure 3. A flow diagram of doping process.

2.3. Doping process

The dopant ions are distributed to DNA almost randomly assuming that the binding probabilities of the dopant to G-C, A-T and $(PO^4)^-$ are similar (33%) in contrast to Dugasani et al. [19].

The number of hydrogen atoms that connects base pairs affects the magnetic phase of M-DNA by changing concentration of metal ions doped to B-DNA [26, 27]. Selection of DNA bases will be investigated and is based on G-C ratio since it includes three hydrogen atoms, while A-T has two bounds of hydrogen. Therefore, G-C ratio of selected DNA is changing from 40.8 to 69.5% to reveal the effect of G-C ratio on doping process and magnetic behaviour.

In the light of recent experimental studies [26–30], dopant ions have different probabilities on where they will bind. **Figures 4** and **5** illustrate the highest probabilities of Cr^{3+} positioning through the DNA helical structure. Hydrogen bind N-N or N-O or N-C atoms existed on the inner edge of pairs of helical structure and have critical importance since researchers

mainly say that dopant ion is actually replaced by hydrogen. So, Cr^{3+}ions are located instead of hydrogen binding to a base pair randomly during doping process for a desired value of doping ratio. Flow diagram in **Figure 3** shows the doping process precisely. In **Figure 4**, dash circles represent the probable positions of doped ion, removing relevant hydrogen in G-C and A-T pair, respectively. Also, dopant ion Cr^{3+} binds to phosphate, as illustrated in **Figure 5**. There are probable positions where dopant ions will be located. It is thought that unbounded oxygen of phosphate holds on to the dopant ion according to Dugasani et al. [19]. Other transition metals (Mn, Fe, Co, Ni and Cu) can be doped to DNA, and they can show ferromagnetic behaviour [19, 26].

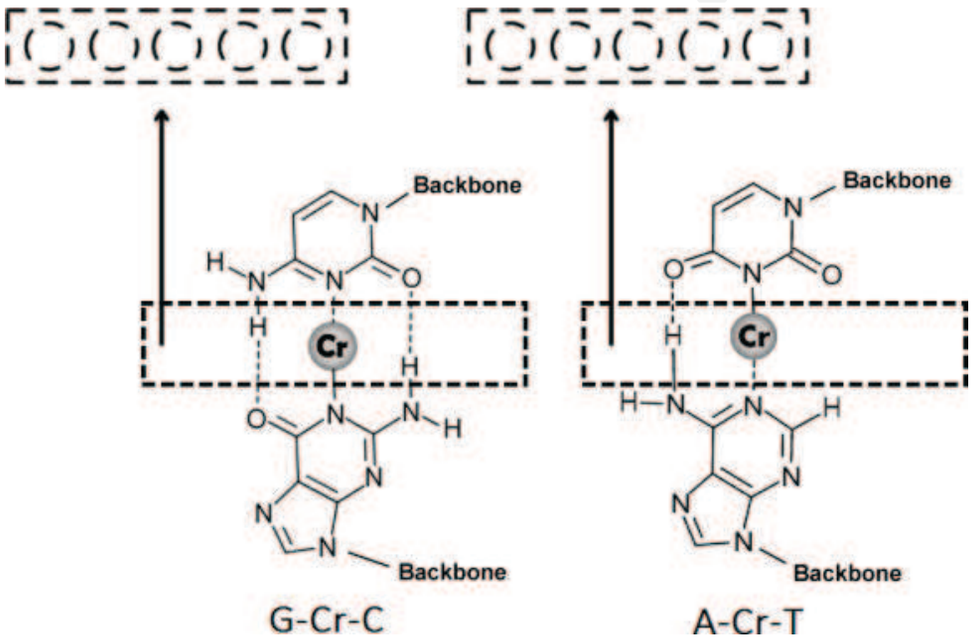

Figure 4. An illustration of probable positions of dopant Cr located instead of hydrogen atom. Dashed circles indicate the possible locations, while grey circle is the most probable one between G-C and A-T base pairs.

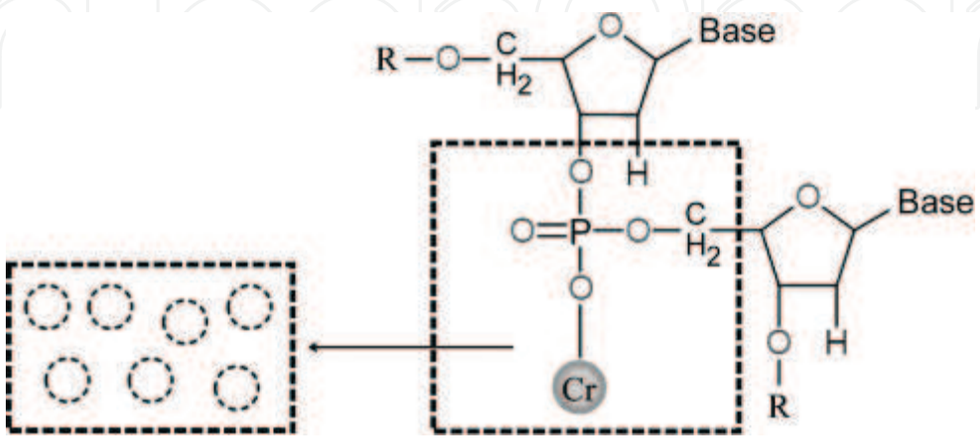

Figure 5. An illustration of probable positions of dopant Cr binding to $(PO_4)^-$. Dashed circles indicate the possible locations, while the grey circle is the most probable one.

3. Simulating the hysteresis

The relationship between applied magnetic field and magnetization is generally explained by using hysteresis loops in solid state physics. A detailed investigation of the hysteresis loop gives immense information about magnetic properties of the material. Saturation magnetization (M_S), described as the maximum value of the magnetization achieved in a sufficiently large magnetic field, can be determined from hysteresis loop. Also, remanent magnetization (M_R), the magnetization that remains in a material when the magnetizing force is zero, and coercive field (H_C), the amount of reverse magnetic field that has to be applied to make the magnetization return to zero, are indicated by hysteresis loop.

Initially, every domain in a ferromagnetic material has an intense magnetization but the whole material is generally unmagnetized because all of the domains are randomly oriented with respect to one another in the absence of magnetic field. The only need is a small external magnetic field to observe ferromagnetism phenomenon. This small magnetic field can cause the magnetic domains to line up with each other and parallel to external magnetic field, the material is now said to be magnetized. In contrast to paramagnets, ferromagnets tend to stay magnetized even if external magnetic field is removed. This tendency is called as "hysteresis". Saturation magnetization, remanent magnetization and coercive field can be viewed in a "*hysteresis loop*" as in **Figure 6**.

3.1. Dipolar Heisenberg Hamiltonian

DNA nanowire is fixed on a glass substrate, and bases adenine, thymine, cytosine and guanine are formed by H, C, O, N, P and dopant Cr^{3+} repeated through z direction in cylindrical coordinates during the simulation process. Glass is chosen because of its non-magnetic property to prevent any external magnetic contribution from another structure except the M-DNA structure since precision in measurement is important. However, doping process affected positions to be changed with little shifts by some perturbations to preserve considerable symmetry and prevent the fall to pieces of the including atoms. The Hamiltonian of the system is described by:

$$\mathcal{H} = -\sum_{<i,j>} J_{\alpha\beta}\left(r_j - r_i\right) S_i^{\alpha} S_j^{\beta} + D \sum_{<i,k>} \left[\frac{S_i^{\alpha} S_k^{\beta}}{r_{ik}^3} - \frac{3\left(S_i^{\alpha} r_{ik}\right)\left(S_k^{\beta} r_{ik}\right)}{r_{ik}^5}\right] - \mu_B g \sum_i B_{\alpha} S_i^{\alpha} \quad (1)$$

where $J_{\alpha\beta}$ is the exchange coupling constant, B_{α} ($\alpha = 0$) is the magnetic field applied along the z-direction, μ_B is the Bohr magneton, and g is the gyromagnetic ratio. α is set to zero to apply external uniform magnetic field through –z direction. The exchange term due to uniqueness and "sole" importance while explaining the strange nature of diluted magnetic semiconductor (DMS) structures is required to be assimilated. This term dipolar Heisenberg Hamiltonian represents the exchange interaction and is related to the distance and type of atoms. It is calculated by summing up nearest neighbours over the whole existed atoms in the system. Theory of diluted magnetic organic structures (DMOS) will be detailed in the next section. The second term factorized by D represents the magnetic dipolar interaction. Even though it can be considered as irrelevant to the subject of chapter, dipole-dipole interaction is also critical to the understanding of magnetic dipoles in optical lattices. The significance of dipolar interac-

http://dx.doi.org/10.5772/67921

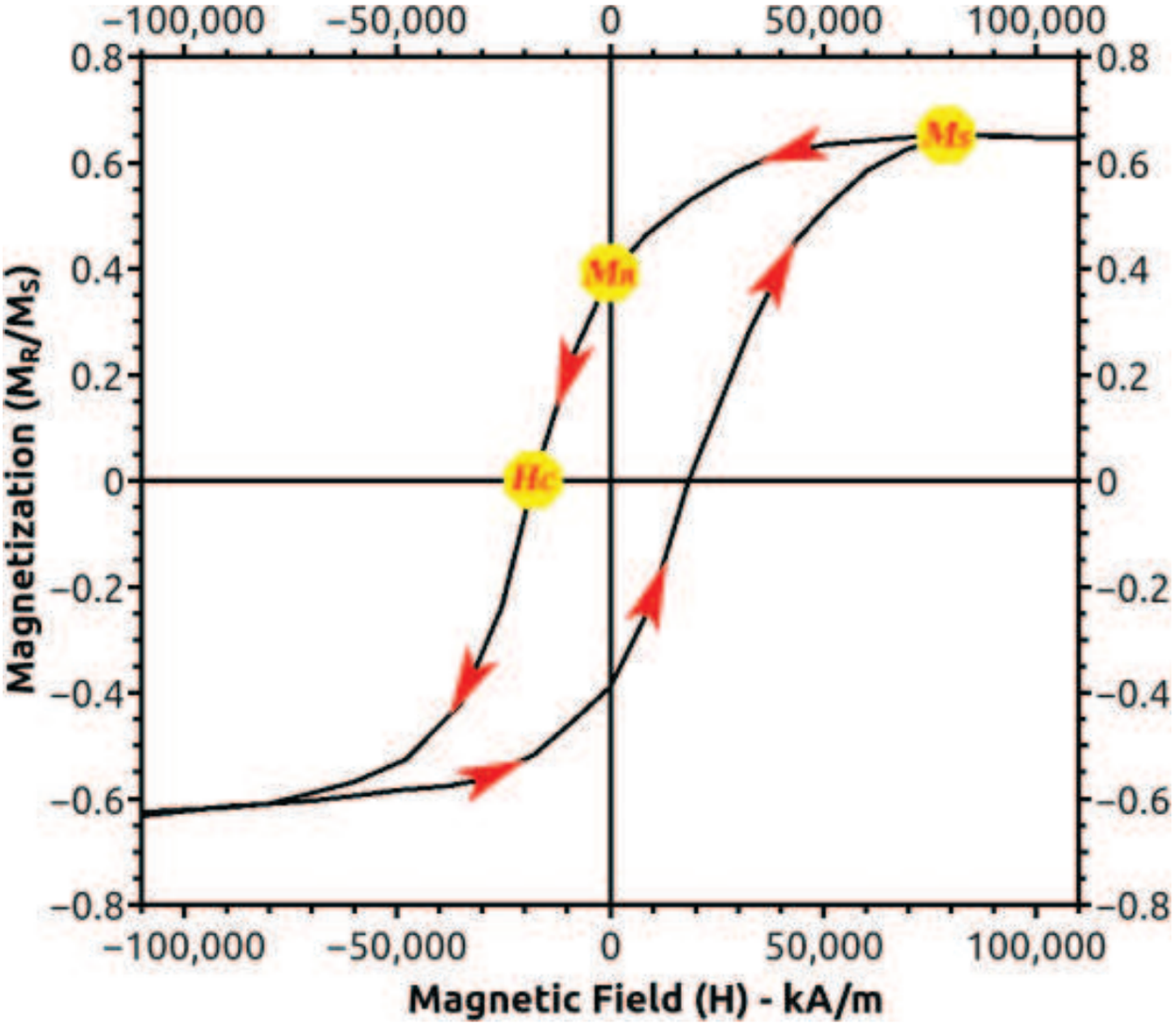

Figure 6. A schematic representation of the hysteresis loop belonging to a ferromagnetic material at a certain temperature (T). H_c= 20,000 (kA/m) and normalized remanent magnetization M_R=0.4.

tion in this theory is intrinsically balancing exchange energy to keep the essence of DMOS dialectic. Finally, the time comes up to talk about the last term, Zeeman energy. The effect of the external field is implicated as the Zeeman energy term by choosing an easy axis for the applied magnetic field. Heisenberg Hamiltonian, as a well-known Hamiltonian, is widely and greatly studied not only in modelling magnetic systems but also there is a distinct scientific "accent" in this theory named diluted magnetic organic structures based on the DMS theory mentioned in [31].

3.2. Theory of diluted magnetic organic structures

Theory of DMOS consists of two basic emphasis on the base of exchange interaction between first 10 nearest neighbours of A, T, C and G atoms in M-DNA helical. First is about the distance-dependent behaviour which means that effect of $J_{\alpha\beta}$ will decrease when distance between interacting neighbours increase. $J_{\alpha\beta} \propto \frac{\delta}{r}$; δ is any positive scalar. The other is that the

major assumption of the theory provides a fundamental essence diverging from superexchange (Kramers-Anderson superexchange), Ruderman–Kittel–Kasuya–Yosida (RKKY) and similar ones. Even if the former can be easily understood, one can deal with the second to perceive it properly. The coupling strength of the atoms between the ions and organic atoms is scaled to the ion-ion coupling strength. That was so fast. Let us start again. Consider an exchange interaction that exists between a random determined X (C, H, O, N, P and Cr^{3+}) and Y (C, H, O, N, P and Cr^{3+}). If X and Y are both Cr^{3+}, the interaction type will be anti-ferromagnetic. However, if X and Y are both organic atoms, $J_{\alpha\beta}$ will vanish because extra soft magnetic contribution by organic atoms should be neglected. Lastly, if X (Y) is organic and Y (X) is Cr^{3+}, they will interact as ferromagnetic. Eq. (2) formulizes the mentioned assumption clearly.

$$J_{\alpha\beta}(r) = \begin{cases} -1 & \alpha = \beta = Cr \\ 0 < J(r) \ll 1 & \alpha = Cr,\ \beta = organic \\ 0 & \alpha = organic,\ \beta = organic \end{cases} . \tag{2}$$

According to a theory, the FM interaction between AFM Cr^{3+} ions and organic atoms, besides $J_{\alpha\beta,}$ vanishes for the organic type of atoms. Furthermore, the system will be aware of the anti-ferromagnetic interaction between Cr^{3+}ions. Actually, Duru et al. [21, 31] proposed a very similar method for the interacting atoms of diluted magnetic semiconductors.

In order to investigate effect of interactions between Cr-Cr and Cr-X (X = C, P, H, N and O) ions on magnetic behaviour, the authors have tried different J-coupling constants. During the simulation process, a reasonable exchange coupling constant between the above-mentioned atoms is traced. The aim is providing consistent characteristic results of the experimental studies.

3.3. MCMC simulation method

Markov chain Monte Carlo (MCMC) simulation method based on the metropolis algorithm is explained by defining an organic lattice introduced is Section 2. Metropolis algorithm [32] uses a transition probability related to energy difference between the first and trial state generated randomly. The ordered structured is formed by Monte Carlo method and also is stochastic due to the nature of the methodology. This time-dependent behaviour is defined by a basic equation in stochastic models like Ising model [33]. Eq. (3) shows:

$$\frac{\partial P_n(t)}{\partial t} = -\sum_{n \neq m} \left[P_n(t) W_{n \to m} - P_m(t) W_{m \to n} \right] \tag{3}$$

Actually, P_n is the probability of the state n at a known finite temperature, t and energy E_n.

$$P_n(t) = \frac{e^{-\frac{E_n}{k_B T}}}{Z} \tag{4}$$

Z denotes the partition function. $W_{n \to m}$ represents the transition probability from state n to state m. In the balance condition, $P_n(t) W_{n \to m} = P_m(t) W_{m \to n}$ will be valid since $\frac{\partial P_n(t)}{\partial t} = 0$. It is known as "detailed balance" [34]. Since it is hard to defeat the problem of partition function Z, one should construct a Markov chain [35]: The new state will be generated by the former state.

Therefore, Z became unnecessary and

$$\frac{P_n(t)}{P_m(t)} = \frac{e^{-\frac{E_n}{k_B T}}}{e^{-\frac{E_m}{k_B T}}} = e^{-\frac{E_n - E_m}{k_B T}} \tag{5}$$

$$\Delta E = E_n - E_m \tag{6}$$

Any transition probability agreed with detailed balance should be accepted. The first selection probability in statistical physics is the metropolis algorithm.

$$W_{m \to n} = \begin{cases} \frac{1}{\tau} e^{-\frac{\Delta E}{k_B T}}, & \Delta E > 0 \\ \frac{1}{\tau}, & \Delta E < 0 \end{cases} \tag{7}$$

τ, denotes the time which is required for a spin flip. Besides the ordinary Monte Carlo, it is transformed to a transition probability to avoid the partition function and in a natural way to take us to a well-known form, Markov chain. Expectation value of an observable A should be calculated by $< A > = \sum_n^N A_n P_n$. However, mean value of magnetization can be easily calculated by $< M > = \frac{1}{N} \sum_i^N S_i$. Flow diagram details the simulation process explicitly, which is shown in **Figure 7**. First, a random atom of the M-DNA nanowire is selected to calculate its energy as described by dipolar Hamiltonian. Second, this step is followed by determining a random magnetic moment of the relevant atom in 3D vector space. Simulation world is calling this state as a trial state. Once again, an energy calculation via to trial state is performed to determine the difference between the trial and former one. Then, the system can decide the

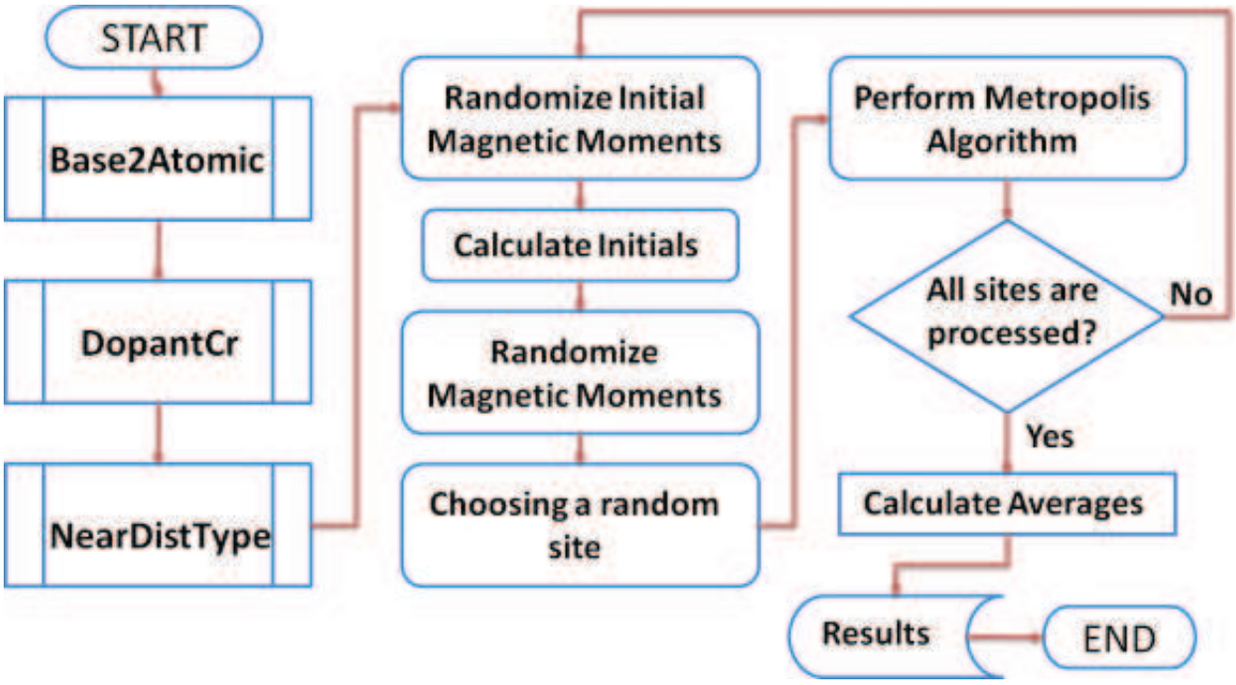

Figure 7. A flow diagram of the simulation process.

new state that will be exist according to the minimization of the energy ($\Delta E < 0$). What if the energy difference is bigger than zero? The answer is Boltzmann statistics. If $\Delta E > 0$, a pseudo random number will be generated and compared with $e^{-\frac{\Delta E}{k_B T}}$. If random number is bigger than $e^{-\frac{\Delta E}{k_B T}}$, trial state will be the new state. In this equation, beta is the inverse temperature included in Boltzmann factor k_B.

4. Magnetic measurements

Magnetic behaviour of materials strongly depends on temperature. Even if magnetic moments are coupled to each other in ferromagnetic materials, thermal agitations can cause random alignment of the magnetic moments in certain temperatures. The thermal agitations tend to keep the atomic moments pointed at random. The result is only partial alignment in the field direction and therefore a small positive susceptibility. The effect of an increase in temperature is an increase of the randomizing effect of thermal agitation that decreases the susceptibility. There is a maximum temperature for all ferromagnets for the disappearance of ferromagnetic property as a result of thermal energy. This critical temperature is called as "Curie temperature". Thermal agitation becomes dominant compared to molecular field upward of Curie temperature. For example, Curie temperatures of iron and cobalt are 1043 and 1400 Kelvin, respectively. Thermal stability of a magnetic material is required to use the material in technological applications. Therefore, determining magnetic properties of a material in different temperatures is the crucial point for the material being a candidate for technological purposes. For our case, room temperature ferromagnetism is the subject so hysteresis loops are measured at room temperature. Magnetization-temperature (M-T) graphs and hysteresis curves of M-DNA can be found in this topic.

4.1. Magnetization-temperature

Two modes are possible for M-T measurements: Zero field cooling (ZFC) and field cooling (FC). In ZFC, the sample is cooled without any applied magnetic field to the desired temperature. Then, the data are collected while heating with certain value of applied magnetic field. In FC, the sample is cooled with some applied magnetic field to the desired temperature. Then, the temperature is increased in the same applied magnetic field. The data can be collected while either the cooling or heating process. The field cooling magnetization-temperature measurement of various samples of M-DNA can be found in **Figures 8** and **9**.

Duru et al. [31] proposed a decrement in the remanent magnetization of the system at temperature $k_B T = 0.01$, from $x = 0.15$ to 0.30, which can be seen in **Figure 8**. The magnetic behaviour of the system strongly depends on the doping ratio (x) because of changing the number of ferromagnetic interactions between the atoms. When a doped atom has all host atomic neighbours, the amount of ferromagnetic coupling for the interacting doped host atoms reaches a maximum. In contrast, decreasing the number of doped-host neighbours and increasing the number of doped-doped neighbours cause the disappearance of ferromagnetism. At the same time, thermal agitations play a well-known role in magnetic systems, especially providing disordered states. A detailed discussion about the effect of doping ratio will be carried out with the information provided by hysteresis curves in the next topic.

http://dx.doi.org/10.5772/67921

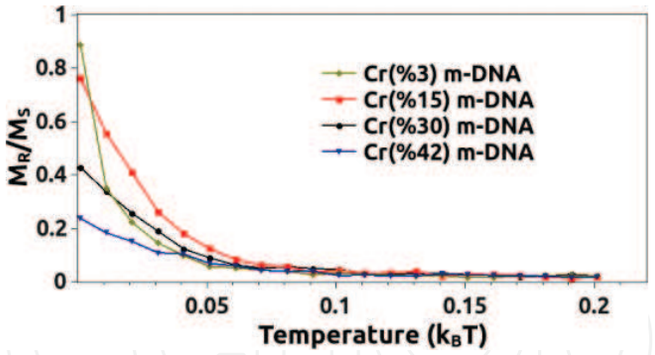

Figure 8. FC of Cr-doped DNA with different doping ratios: 3, 15, 30 and 42%. M_R/M_S ratio of 15%-doped M-DNA is larger when compared to 3, 30 and 42% at 0.02 k_BT.

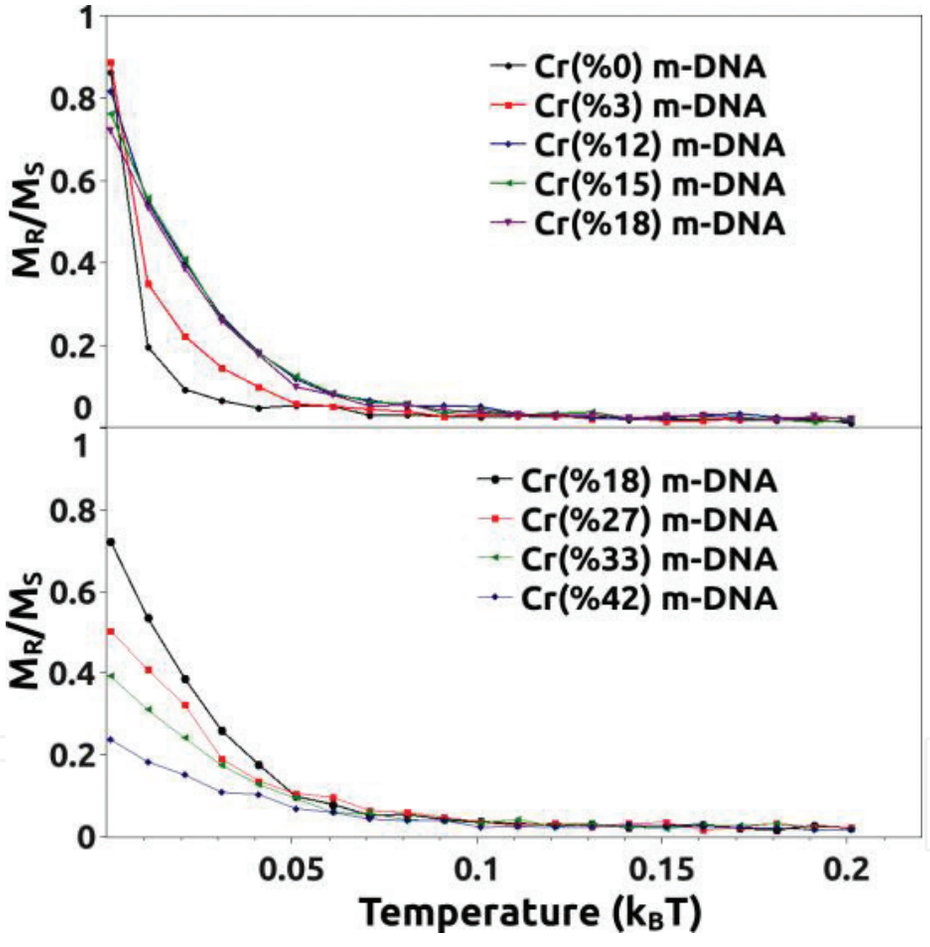

Figure 9. FC of M-DNA doped by Cr **(a)** 0, 3, 12, 15 and 18% **(b)** 18, 27, 33 and 42%.

4.2. Hysteresis curves

The idea of using DNA, a natural nanowire, in magnetism-based technological applications arose when the first paramagnetic resonance signal was observed by Bliumenfeld and Bendersky [36]. The signal explicitly revealed that B-DNA is a paramagnetic material. A hysteresis curve of B-DNA verifies its paramagnetic phase as shown in **Figure 10**. The outputs of the simulation process for B-DNA were also used to calibrate the main parameters of the doped-DNA systems [31].

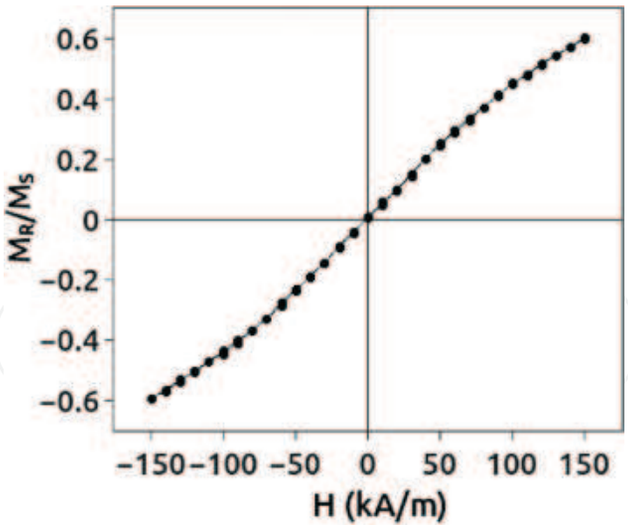

Figure 10. Hysteresis loop of B-DNA at $k_BT/J=0.02$.

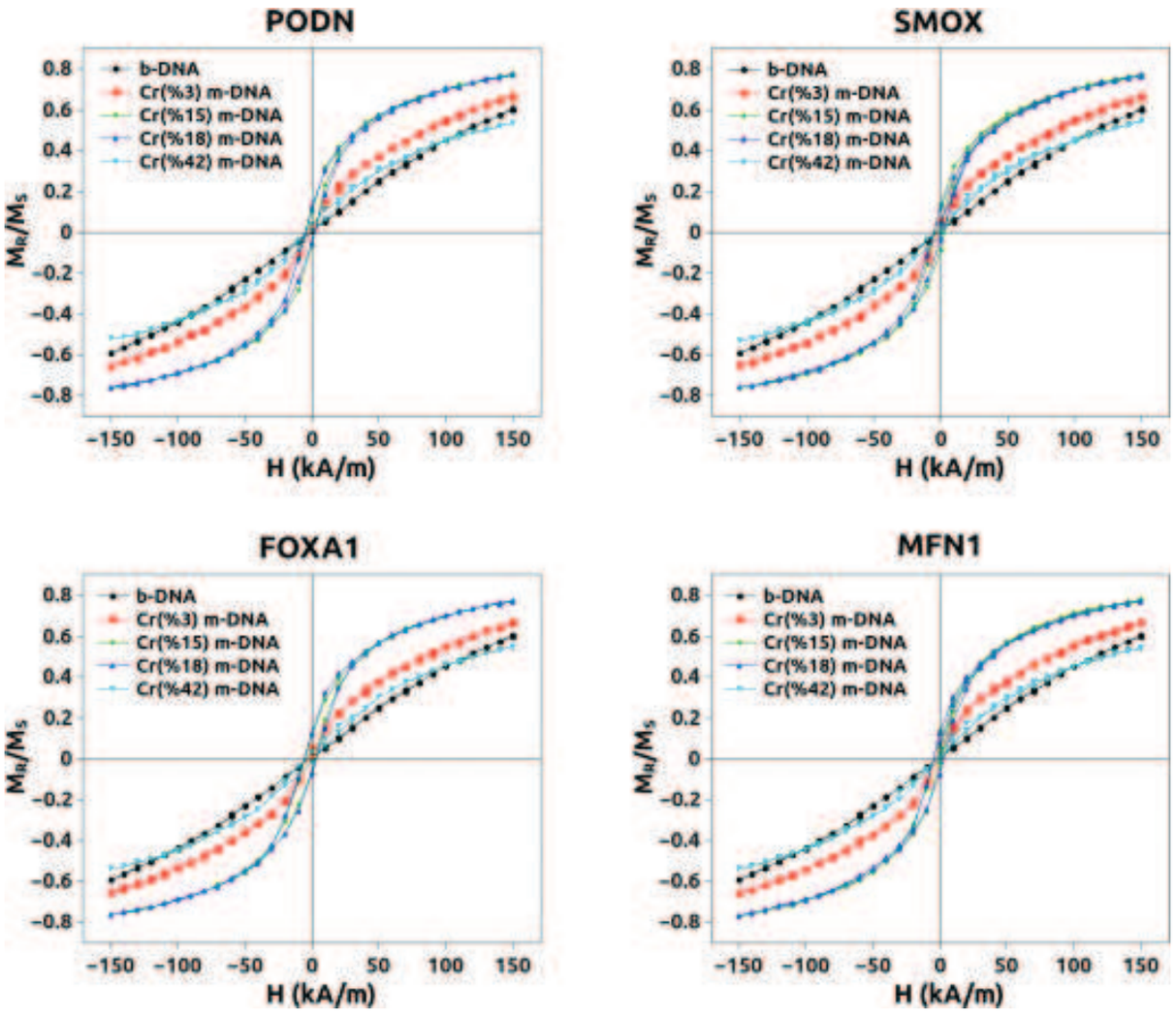

Figure 11. Hysteresis curves of B-DNA and Cr-doped M-DNA at 3, 15, 18 and 42% ratio for PODN, SMOX, FOXA1 and MFN1 gene sequences. The difference between hysteresis loops of various genes is negligible.

Although the Curie temperature of M-DNA is not so far from room temperature, **Figure 11** makes it clear that Cr-doped M-DNA has a relatively higher coercivity for $x = 0.15$ against other organomagnetic materials [37]. It is supposed that higher Cr concentrations larger than 15% lead the system to a state of disorder. Decrement in the M_R and coercive field indicates a change in the magnetic phase of DNA with increasing the doping ratio after $x = 0.15$ [31]. Briefly, the system has nonlinear phase transition behaviour with increasing the doping ratio from 0 to 42%: first, it is paramagnetic as in B-DNA and then gains soft ferromagnetic and antiferromagnetic properties, respectively.

Particularly, residual magnetism in system vanishes for $x = 0.42$, indicating that the ferromagnetic behaviour of the system completely vanishes due to AFM ion coupling, while there is no significant difference between $x = 0.15$ and 0.18 because of the random distribution of the Cr ions.

When **Figure 12** is roughly skimmed, DMOS behaviour should be understood easily. Remanent magnetization normalized by saturation magnetization has the bigger value near to 15% doping ratio and decreases with increasing doping ratio. Hysteresis and remanent magnetization figures of only four different genes of the sample group are implemented to this section since it is sufficient to verify the theory.

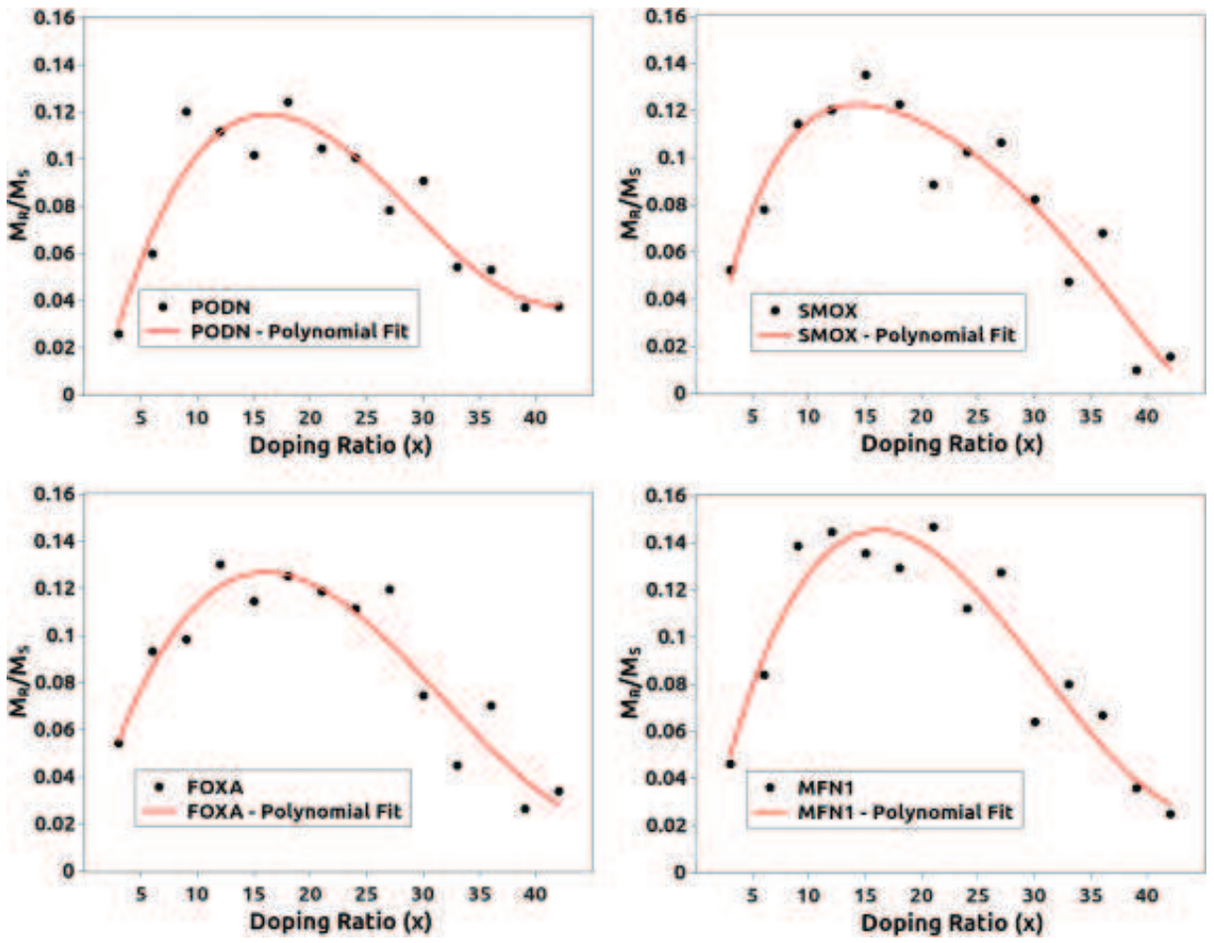

Figure 12. M_R/M_S MR/MS versus doping ratio of Cr-doped M-DNA for PODN, SMOX, FOXA1 and MFN1 gene sequences. The presentation of changing magnetic phase is supported by second-order polynomial fitting to have a clear understanding.

5. Summary

Geometrical structure of B-DNA nanowire in Euclidian space is generated by a given sample set of genes, including non-dispersive base sequences that consist of certain G-C ratio. The modifying process of B-DNA nanowire by doping Cr^{3+} ions is explained clearly and detailed by flow diagram as made from the simulation process of the whole system. However, MCMC method based on metropolis algorithm is used to mimic M-DNA nanowire to discover a proper Hamiltonian in the case of DMOS theory. Existence of a ferromagnetic interaction between Cr-X (X = N, H, O, P and C) and an anti-ferromagnetic interaction between Cr-Cr neighbouring atoms underlies the theory with Heisenberg Hamiltonian-included dipolar interaction. Moreover, hysteresis curves and remanent magnetization versus doping ratio of Cr is presented after critical temperature is determined by simulating of FC. $k_B T/J$ ratio is set to ~0.1 after several trials to calibrate parameters according to the paramagnetic behaviour. Duru et al. proposed a decrement in the remanent magnetization of the system at temperature $k_B T$ = 0.01 from x = 0.15 to 0.30. Moreover, hysteresis curves reveal the DMS characteristic of M-DNA by Cr^{3+}, and it is not crucially dependent to type of atom. Different type of atom should only change coercive field or doping ratios that system gains ferromagnetic property. One must not forget that the dopants must have conducting property such as metals or semi-conductors.

Acknowledgements

We would like to thank the Scientific Research Commission (BAPKO) of Marmara University supporting this chapter under the research project numbered FEN-A-100616-0275.

Author details

Caner Değer[1], Vahap Eldem[2] and İzzet Paruğ Duru[1]*

*Address all correspondence to: izzetparug.duru@marun.edu.tr

1 Department of Physics, Marmara University, İstanbul, Turkey

2 Department of Biology, İstanbul University, İstanbul, Turkey

References

[1] Dugasani SR, Park B, Gnapareddy B, Pamanji SR, Yoo S, Lee KW, Lee S, Jun SC, Kim JH, Kim C, Park SH. Tunable near white light photoluminescence of lanthanide ion (Dy^{3+}, Eu^{3+} and Tb^{3+}) doped DNA lattices. RSC Advances. 2015;**5**(69):55839-55846. DOI: 10.1039/C5RA07360J

[2] Göhler B, Hamelbeck V, Markus TZ, Kettner M, Hanne GF, Vager Z, Naaman R, Zacharias H. Spin selectivity in electron transmission through self-assembled monolayers of double-stranded DNA. Science. 2011;**331**(6019):894-897. DOI: 10.1126/science.1199339

[3] Steckl AJ. DNA—a new material for photonics? Nature Photonics. 2007;**1**:3-5. DOI: 10.1038/nphoton.2006.56

[4] Nam J-M, Thaxton CS, Mirkin CA. Nanoparticle-based bio-bar codes for the ultrasensitive detection of proteins. Science. 2003;**301**(5641):1884-1886. DOI: 10.1126/science.1088755

[5] Lu Y, Goldsmith BR, Kybert NJ, Johnson ATC. DNA-decorated graphene chemical sensors. Applied Physics Letters. 2010;**97**(8). DOI: 10.1063/1.3483128

[6] Hu J-F (胡建芬), Feng L (冯琳), Zhang W-X (张文星), Li Y (李勇), Lu Y-X (卢亚鑫). Detection of DNA bases using Fe atoms and graphene. Chinese Physics Letters. 2016;**33**(1). DOI: 10.1088/0256-307X

[7] Azbel MY. Phase transitions in DNA. Physical Review A. 1979;**20**(4):1671-1684. DOI: 10.1103/PhysRevA.20.1671

[8] Alivisatos AP, Johnsson KP, Peng X, Wilson TE, Loweth CJ, Bruchez MP Jr, Schultz PG. Organization of "nanocrystal molecules" using DNA. Nature. 1996;**382**:609-611. DOI: 10.1038/382609a0

[9] Mirkin CA, Letsinger RL, Mucic RC, Storhoff JJ. A DNA-based method for rationally assembling nanoparticles into macroscopic materials. Nature. 1996;**382**:607-609. DOI: 10.1038/382607a0

[10] Braun E, Eichen Y, Sivan U, Ben-Yoseph G. DNA-templated assembly and electrode attachment of a conducting silver wire. Nature. 1998;**391**:775-778. DOI: 10.1038/35826

[11] Richter J, Mertig M, Pompe W, Mönch I, Schackert HK. Construction of highly conductive nanowires on a DNA template. Applied Physics Letters. 2001;**78**(4). DOI: 10.1063/1.1338967

[12] Park SJ, Taton TA, Mirkin CA. Array-based electrical detection of DNA with nanoparticle probes. Science. 2002;**295**(5559):1503-1506. DOI: 10.1126/science.1067003

[13] Keren K, Berman RS, Buchstab E, Sivan U, Braun E. DNA-templated carbon nanotube field-effect transistor. Science. 2003;**302**(5649):1380-1382. DOI: 10.1126/science.1091022

[14] Yi J. Emergent paramagnetism of DNA molecules. Physical Review B. 2006;**74**(21):212406. DOI: 10.1103/PhysRevB.74.212406

[15] Savin AV, Mazo MA, Kikot IP, Manevitch LI, Makoto AVO. Heat conductivity of the DNA double. Physical Review B. 2011;**83**(24):245406. DOI: 10.1103/PhysRevB.83.245406

[16] Sakamoto H, Mizoguchi K. Electronic states of DNA and M-DNA studied by optical absorption. Physical Review E. 2014;**89**(2):022719. DOI: 10.1103/PhysRevE.89.022719

[17] Panahi M, Chitsazanmoghaddam M. Comment on "modeling the electrical conduction in DNA nanowires: Charge transfer and lattice fluctuation theories". Physical Review E. 2016;**93**(4):046401. DOI: 10.1103/PhysRevE.93.046401

[18] Behnia S, Fathizadeh S. Modeling the electrical conduction in DNA nanowires: Charge transfer and lattice fluctuation theories. Physical Review E. 2015;**91**(2):022719. DOI: 10.1103/PhysRevE.91.022719

[19] Dugasani SR, Lee N, Lee J, Kim B, Hwang SU, Lee KW, Kang WN, Park SH. Magnetic characteristics of copper ion-modified DNA thin films. Scientific Reports. 2013;**3**(1819). DOI: 10.1038/srep01819

[20] Nikiforov VN, Kuznetsov VD, Yevdokimov YM, Irkhind VY. Magnetic properties of Gd^{3+} ions in the spatially distributed DNA molecules. Journal of Magnetism and Magnetic Materials. 2014;**368**:338-341. DOI: 10.1016/j.jmmm.2014.06.008

[21] Duru IP, Değer C, Eldem V, Kalayci T, Aktas S. Theory of room temperature ferromagnetism in Cr modified DNA nanowire. Journal of Physics D: Applied Physics. 2016;**49**:135004. DOI: 10.1088/0022-3727/49/13/135004

[22] van Dijk M, Bonvin AMJJ. 3D-DART: A DNA structure modelling server. Nucleic Acid Research. 2009;**37**(2). DOI: 10.1093/nar/gkp287

[23] Utrecht Biomolecular Interaction Web Portal. 3DDART@BonvinLab [Internet]. Available from: http://milou.science.uu.nl/services/3DDART/

[24] Watson CD, Crick FHC. Molecular structure of nucleic acids. Nature. 1953;**4356**:737

[25] Franklin R, Gosling RG. The structure of sodium thymonucleate fibres. II. The cylindrically symmetrical Patterson function. Acta Crystallographica. 1953b;**6**:678-685. DOI: 10.1107/S0365110X53001940

[26] Dugasani SR, Kim M, Lee I-y, Kim JA, Gnapareddy B, Lee KW, Kim T, Huh N, Kim G-H, Park SC. Construction and characterization of Cu^{2+}, Ni^{2+}, Zn^{2+}, and Co^{2+} modified-DNA crystals. Nanotechnology. 2015;**26**(27):275604. DOI: 10.1088/0957-4484/26/27/275604

[27] Mizoguchi K. Physical properties of natural DNA and metal ion inserted M-DNA. In: Heckman EM, Singh TB, Yoshida J, editors. Proceedings of SPIE. Nanobiosystems: Processing, Characterization, and Applications; 2008. DOI: 10.1117/12.801478

[28] Dong R, Yan X, Li K, Ban G, Wang M, Cui S, Yang B. Effects of metal ions on conductivity and structure of single DNA molecule in different environmental conditions. Nanoscale Research Letters. 2010;**5**:1431. DOI: 10.1007/s11671-010-9657-3

[29] Park H-Y, Dugasani SR, Kang D-H, Jeon J, Jang SK, Lee S, Roh Y, Park SH, Park J-H. n- and p-type doping phenomenon by artificial DNA and M-DNA on two-dimensional transition metal dichalcogenides. ACS Nano. 2014;**8**(11):11603-11613. DOI: 10.1021/nn5048712

[30] Joseph J, Schuster GB. Long-distance radical cation hopping in DNA: The effect of thymine−Hg(II)−thymine base pairs. Organic Letters. 2007;**9**(10):1843-1846. DOI: 10.1021/ol070135a

[31] Duru İP, Değer C, Kalaycı T, Arucu M. A computational study on magnetic effects of Zn Cr O 1−x x type diluted magnetic semiconductor. Journal of Magnetism and Magnetic Materials. 2015;**396**:268-274. DOI: 10.1016/j.jmmm.2015.08.031

[32] Metropolis N, et al. Journal of Chemical Physics. 1953;**21**:1087

[33] Kawasaki K. In: Domb C, Green MS, editors. Chapter 4.Mode Coupling and Critical Dynamics. Phase Transitions and Critical Phenomena. Vol. 5. London: Academic Press; 1976

[34] Boltzmann L. Lectures on Gas Theory. Berkeley, CA, USA: University of California Press; 1964

[35] Hastings WK. Monte Carlo sampling methods using Markov chains and their applications. Biometrika. 1970;**57**(1):97-109. DOI: 10.1093/biomet/57.1.97. JSTOR 2334940. Zbl 0219.65008

[36] Bliumenfeld LA, Bendersky VA. Magnetic and Dielectric Properties of High-ordered Macromolecular Structures. Doklady Akademii Nauk, SSSR. 1960;133:1451-1454

[37] Jain R, Kabir K, Gilroy JB, Mitchell KAR, Wong K, Hicks RG. High-temperature metal–organic magnets. Nature. 2007;**445:**291-294

IntechOpen